NONLINEAR WAVE PRESSURES GIVEN BY EXTREME WAVES ON AN UPRIGHT BREAKWATER: THEORY AND EXPERIMENTAL VALIDATION

Alessandra Romolo[1] and Felice Arena[2]

An analytical nonlinear theory is presented for the interaction between three-dimensional sea wave groups and a seawall during the occurrence of an exceptionally high crest or deep trough of the water elevation. The solution to the second order of the free surface displacement and of the velocity potential is derived by considering an irrotational, inviscid, incompressible flow bounded by a horizontal seabed and a vertical impermeable seawall. The analytical expression of the nonlinear wave pressure is derived. The resulting theory is able to fully describe the mechanics at the seawall and in front of it, which represents a strongly nonhomogeneous wave field, then demonstrating that it is influenced by characteristic parameters and wave conditions. The theoretical results are in good agreement with measurements carried out during a small-scale field experiment at the Natural Ocean Engineering Laboratory in Reggio Calabria (Italy). The theoretical and experimental comparisons show that some distinctive phenomena regarding wave pressures of very high standing wave groups at a seawall, in the absence of either overturning or breaking waves, may be associated with nonlinear effects.

Keywords: seawall; reflection; nonlinear wave groups.

INTRODUCTION

Early studies on nonlinear standing sea waves in irrotational flow focused on periodic gravity waves. Penny and Price (1952) calculated a numerical solution up to the fifth order for the two-dimensional case in infinite depth through a perturbation series, using the wave amplitude as a small parameter. The solution provided important information about the shape of the highest crests of the water surface that was in agreement with later experiments of Taylor (1953), Fultz (1962). By considering standing waves on a finite depth fluid, Tadjbakhsh and Keller (1960) developed a third-order perturbation series, and Goda (1967) later extended the series up to the fourth order. In subsequent research that considered sea waves of finite amplitude, several solutions were found using different approaches. A complete review of the literature dealing with nonlinear water waves, including standing waves, is given in Schwartz and Fenton (1982). Tsai and Jeng (1994) defined a Fourier series for a finite water depth. Schultz *et al.* (1998) considered a time-marching spectral boundary integral method for potential flow to obtain a highly accurate resolution that takes into account both the gravity and surface tension.

Moreover, considering the behaviour of wave pressures acting on a seawall when extreme waves are realised at the structure the basic studies have been investigated the formation of falling vertical jets at the seawall that are caused by either overturning or breaking waves. This problem was investigated by Jiang *et al.* (1996), Longuet-Higgins (2001), Longuet-Higgins and Dommermuth (2001) and Cooker and Peregrine (1995).

On the whole, it has been proved that the mechanics of sea waves impacting a seawall can be well described by a wave model of irrotational, inviscid, incompressible flow, as was explained in a complete review of the phenomenon by Peregrine (2003). However, few contributions are found in the literature that consider the mechanics of nonlinear irregular sea waves in the absence of overturning or breaking waves.

Diffracted random wave fields with a linear approach have more recently been analyzed by Ohl *et al.*(2001), Walker and Eatock Taylor (2005), and Arena (2006; see also Romolo *et al*., 2009) analysed the interaction between random wave groups interacting with a horizontal submerged cylinder.

Boccotti (1982, 2000) proposed the linear quasi-determinism (QD) theory for the highest sea waves in a Gaussian sea. The QD is able to describe the mechanics of three-dimensional wave groups when a very high sea wave occurs, and it can be applied to both homogeneous and nonhomogeneous wave fields. For random sea waves in an undisturbed field, a number of models that are exact to the second order in a Stokes expansion are given by Sharma and Dean (1981). For wave groups propagating in an undisturbed wave field, the QD theory was extended to the second order by Arena (2005) and Arena *et al*. (2008). Boccotti (1997, 2000) applied his linear theory to investigate the mechanics of sea wave groups interacting with a reflective seawall. Later, Romolo and Arena (2008, 2010) derived a correction of this theory up to the second order for the case of long-crested (two-dimensional) sea wave groups.

[1] Natural Ocean Engineering Laboratory, Dept. MecMat, *Mediterranea* University, Loc. Feo di Vito, Reggio Calabria, 89122, Italy; aromolo@unirc.it
[2] Natural Ocean Engineering Laboratory, Dept. MecMat, *Mediterranea* University, Loc. Feo di Vito, Reggio Calabria, 89122, Italy; arena@unirc.it

The paper presents a close-form solution to this theory, up to the second order, for three-dimensional (short-crested) sea wave groups interacting with a seawall during the occurrence of an exceptionally high crest or deep trough of water elevation. One of the most important results of the second-order theory discussed in this paper concerns the behaviours of wave pressures when either the highest crest or the deepest trough of the water surface impacts the structure. In order to validate the proposed theory up to the second order for wave groups in reflection, a small-scale field experiment on an upright seawall was carried out at the Natural Ocean Engineering Laboratory in Reggio Calabria (Italy). The results of the experiment shown a good confirmation of the analytical predictions.

ANALYTICAL MODEL

The linear quasi-determinism theory for wave groups in reflection

When an extremely high individual crest of given height H_C occurs at a fixed point $\underline{x}_0 \equiv (x_0, y_0)$ at time instant t_0 in a random wind-generated sea state, which is assumed to be a stationary as well as a Gaussian process of time, the first formulation of the quasi-determinism theory (Boccotti 1982, 2000) allows us to predict, with very high probability, the expected configuration of the wave field in the time domain, before and after t_0, and in the space domain, in the area surrounding $\underline{x}_0$.

Under the assumption that H_C is very high with respect to the standard deviation σ of the wave field where it is realized (that is to say $H_C/\sigma \to \infty$), the theory proves that the configuration of the water surface tends, with a probability approaching 1, to assume a well-defined average feature in space and time,

$$\bar{\eta}(\underline{x}_0 + \underline{X}, t_0 + T) = H_C \frac{\Psi(\underline{X}, T)}{\Psi(\underline{0}, 0)}, \tag{1}$$

which is associated with the following velocity potential:

$$\bar{\phi}(\underline{x}_0 + \underline{X}, z, t_0 + T) = H_C \frac{\Phi(\underline{X}, z, T)}{\Psi(\underline{0}, 0)}. \tag{2}$$

In Equations (1) and (2), Ψ is the autocovariance of the surface displacement of the random wave field in which the exceptionally high crest elevation occurs and it is defined as

$$\Psi(\underline{X}, T) = < \eta(\underline{x}_0, t)\eta(\underline{x}_0 + \underline{X}, t + T) >, \tag{3}$$

and Φ is the cross-covariance of the surface displacement η and the velocity potential ϕ:

$$\Phi(\underline{X}, z, T) = < \eta(\underline{x}_0, t)\phi(\underline{x}_0 + \underline{X}, z, t + T) >. \tag{4}$$

The main properties of the theory are that it can be applied to a nearly arbitrary bandwidth of the spectrum, and to sea waves propagating either in an undisturbed wave field or in a diffracted wave field.

In this paper, we consider three-dimensional (short-crested) standing sea waves resulting from the full reflection of progressive three-dimensional waves impacting a seawall at an arbitrary angle. Under these conditions, by the application of the quasi-determinism theory (Boccotti 1997, 2000) conditional to the occurrence of the exceptionally high wave crest H_C of the surface elevation at time t_0 at $\underline{x}_0$, which can be either at or in front of the reflective seawall, the linear deterministic solution for the surface displacement at location $(\underline{x}_0 + \underline{X}, z)$ at time instant $t_0 + T$ gives

$$\bar{\eta}_{R_1}(\underline{x}_0 + \underline{X}, t_0 + T) = 4\frac{H_C}{\sigma_R^2}\int_0^{\infty}\int_0^{2\pi} S(\omega, \theta)\cos(kX\sin\theta - \omega T)\cos(k\, y_0\cos\theta)\cos[k(y_0 + Y)\cos\theta]\mathrm{d}\theta\,\mathrm{d}\omega, \tag{5}$$

with the associated velocity potential at level z defined by

$$\bar{\phi}_{R_1}(\underline{x}_0 + \underline{X}, z, t_0 + T) = \frac{4gH_C}{\sigma_R^2}\int_0^{\infty}\int_0^{2\pi} S(\omega, \theta)\frac{\cosh[k(d + z)]}{\omega\,\cosh(kd)}\sin(kX\sin\theta - \omega T)\cos(ky_0\cos\theta)\cos[k(y_0 + Y)\cos\theta]\mathrm{d}\theta\,\mathrm{d}\omega. \tag{6}$$

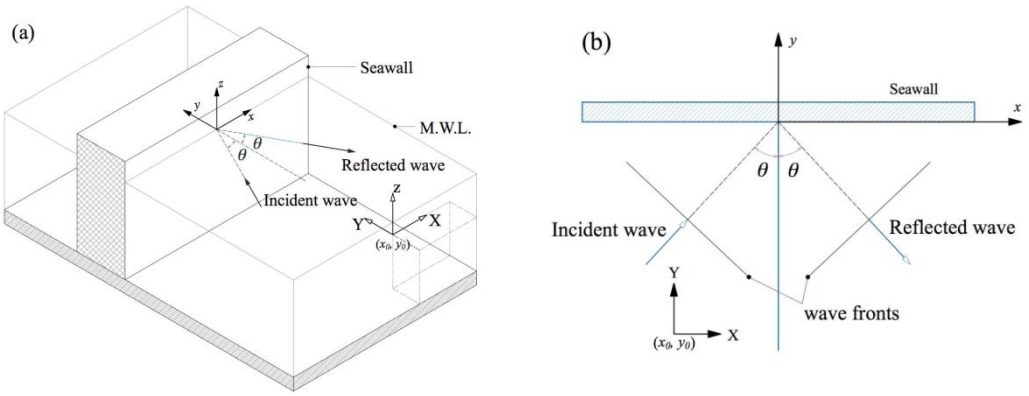

Figure 1: Sketch diagram of three-dimensional wave groups in reflection: axonometric projection (a) and horizontal plan (b). An absolute Cartesian coordinate system (x,z) = (x,y,z) is fixed at the structure and a relative Cartesian coordinate system ($\underline{x}_0$,z) = (x_0,y_0,0) is set at the point at which either an exceptionally high crest or trough amplitude for the surface displacement occurs [$\underline{x}_0$ = 0, if it occurs on the seawall].

Here, g is the acceleration due to gravity, $S(\omega,\theta)$ is the directional wave spectrum of the incident waves, and σ_R^2 is the variance of the surface displacement of the wind-generated wave field in the reflection (which is as a whole assumed to be random, stationary and Gaussian), given by

$$\sigma_R^2 = \sigma_R^2(y_0) = 4\int_0^\infty\int_0^{2\pi} S(\omega,\theta)\cos^2(ky_0\cos\theta)\mathrm{d}\theta\,\mathrm{d}\omega, \tag{7}$$

where wave frequency ω and wavenumber k both satisfy the linear dispersion rule

$$\omega^2 = gk\tanh(kd). \tag{8}$$

Solutions (5) and (6) refer to a frame of reference depicted in Figure 1.

From the linear Bernoulli equation: $\overline{p}_{w_{R_1}} = -\rho\,\partial_T(\overline{\phi}_{1_R})$, the first-order wave pressure acting on the seawall through the quasi-determinism theory is calculated from Equation (6)

$$\overline{p}_{w_{R_1}}(\underline{x}_0+\underline{X},z,t_0+T) = \frac{4\rho g H_C}{\sigma_R^2}\int_0^\infty\int_0^{2\pi} S(\omega,\theta)\frac{\cosh[k(d+z)]}{\cosh(kd)}\cos(kX\sin\theta-\omega T)\cos(ky_0\cos\theta)\cos[k(y_0+Y)\cos\theta]\mathrm{d}\theta\,\mathrm{d}\omega. \tag{9}$$

where ρ denotes the water density.

The second-order solution of wave groups in reflection through the quasi-determinism theory

By adopting the framework of a potential flow in which the fluid is incompressible and inviscid and the flow is irrotational, and by further assuming the fluid in a constant depth *d* bounded by an impermeable seabed and a rigid vertical seawall, the second-order closed-form solution for both the free surface displacement $\overline{\eta}_{2_R}$ and the velocity potential $\overline{\phi}_{2_R}$ has been derived by solving the nonlinear partial differential system given by the continuity equation (Laplace's equation), the kinematics free surface boundary condition, the dynamic free surface boundary condition (the Bernoulli equation), the bottom boundary condition and the wall boundary condition (Romolo and Arena 2008, 2010).

The complete solution for $\overline{\eta}_{2_R}$ and $\overline{\phi}_{2_R}$ (Romolo and Arena 2008, 2010) is given by

$$\overline{\eta}_{2_R}(\underline{x}_0+\underline{X},t_0+T) = \frac{H_C^2}{8\sigma_R^4}\int_0^\infty\int_0^\infty\int_0^{2\pi}\int_0^{2\pi} S(\omega_1,\theta_1)S(\omega_2,\theta_2)\cos(\varphi_1)\cos(\varphi_2)\{[\mathrm{A}_1^-\cos(\alpha_1-\alpha_2)+\mathrm{A}_2^-\cos(\alpha_1+\alpha_2)] \tag{10}$$
$$\cos(\lambda_1-\lambda_2)+[\mathrm{A}_1^+\cos(\alpha_1+\alpha_2)+\mathrm{A}_2^+\cos(\alpha_1-\alpha_2)]\cos(\lambda_1+\lambda_2)\}\,\mathrm{d}\theta_2\,\mathrm{d}\theta_1\,\mathrm{d}\omega_2\,\mathrm{d}\omega_1-\Xi/g$$

$$\overline{\phi}_{2_R}(\underline{x}_0+\underline{X},z,t_0+T) =$$
$$g^2\frac{H_C^2}{8\sigma_R^4}\int_0^\infty\int_0^\infty\int_0^{2\pi}\int_0^{2\pi} S(\omega_1,\theta_1)S(\omega_2,\theta_2)\,\omega_1^{-1}\omega_2^{-1}\cos(\varphi_1)\cos(\varphi_2)\{[\mathrm{C}_1^-\cos(\alpha_1-\alpha_2)+\mathrm{C}_2^-\cos(\alpha_1+\alpha_2)](\omega_1-\omega_2)^{-1} \tag{11}$$
$$\sin(\lambda_1-\lambda_2)+[\mathrm{C}_1^+\cos(\alpha_1+\alpha_2)+\mathrm{C}_2^+\cos(\alpha_1-\alpha_2)](\omega_1+\omega_2)^{-1}\sin(\lambda_1+\lambda_2)\}\,\mathrm{d}\theta_2\,\mathrm{d}\theta_1\,\mathrm{d}\omega_2\,\mathrm{d}\omega_1+\Xi T$$

where H_C is the exceptionally linear high crest elevation, σ_R^2 is expressed by relation (7), and $A_n^{\square}$ and $C_n^{\square}$ (n =1,2) parameters are the so called interaction kernels respectively of the nonlinear free surface and of the velocity potential related to their quadratic transfer functions (the expressions are reported in the Appendix). $S(\omega_n, \theta_n)$ (n =1,2) is the directional wave spectrum of the incident waves and ϕ_n, α_n, λ_n (n =1,2) are defined by relations

$$\begin{aligned} &\varphi_n(k_n,\theta_n,y_0) = k_n y_0 \cos\theta_n \\ &\alpha_n(k_n,\theta_n,y_0,Y) = k_n \cos\theta_n (y_0 + Y) \\ &\lambda_n(k_n,\theta_n,X,T) = k_n \sin\theta_n X - \omega_n T \qquad n = 1,2. \end{aligned} \tag{12}$$

Retaining the terms up to the second-order by the *Bernoulli's equation*, the nonlinear deterministic wave pressure is achieved

$$\begin{aligned} \overline{p}_{w_{2R}}(\underline{x}_0 + \underline{X}, z, t_0 + T) = \rho g^2 \frac{H_{C_R}^2}{2\sigma^4} \Bigg\{ & \frac{1}{4} \int_0^\infty \int_0^\infty \int_0^{2\pi} \int_0^{2\pi} S(\omega_1,\theta_1) S(\omega_2,\theta_2)\, \omega_1^{-1} \omega_2^{-1} \cos(\varphi_1)\cos(\varphi_2) \{[C_1^- \cos(\alpha_1 - \alpha_2) \\ & + C_2^- \cos(\alpha_1 + \alpha_2)]\cos(\lambda_1 - \lambda_2) + [C_1^+ \cos(\alpha_1 + \alpha_2) + C_2^+ \cos(\alpha_1 - \alpha_2)]\cos(\lambda_1 + \lambda_2)\} \, \mathrm{d}\theta_2 \, \mathrm{d}\theta_1 \, \mathrm{d}\omega_2 \, \mathrm{d}\omega_1 \\ & - \sum_{p=1}^{3} \left[\int_0^\infty \int_0^{2\pi} S(\omega_1,\theta_1) \frac{\omega_1^{-1} k_1}{\cosh(k_1 d)} \cos(\varphi_1) Q_p(\underline{x}_0 + \underline{X}, z, t_0 + T; \omega_1, \theta_1) \mathrm{d}\theta_1 \, \mathrm{d}\omega_1 \right]^2 \Bigg\} - \rho \Xi \qquad \text{with } p = 1, 2, 3, \end{aligned} \tag{13}$$

$$Q_p(\underline{x}_0 + \underline{X}, z, t_0 + T; \omega_1, \theta_1) = \begin{cases} \cosh[k_1(d+z)]\sin(\theta_1)\cos(\alpha_1)\cos(\lambda_1) & \text{for } p = 1 \\ -\cosh[k_1(d+z)]\cos(\theta_1)\sin(\alpha_1)\sin(\lambda_1) & \text{for } p = 2 \\ \sinh[k_1(d+z)]\cos(\alpha_1)\sin(\lambda_1) & \text{for } p = 3. \end{cases} \tag{14}$$

In solutions (10), (11) and (13), the parameter Ξ is expressed by relation

$$\Xi = -g \frac{H_{C_R}^2}{8\sigma^4} \int_0^\infty \int_0^\infty \int_0^{2\pi} \int_0^{2\pi} S(\omega_1,\theta_1) S(\omega_2,\theta_2) \frac{2k_1}{\sinh(2k_1 d)} \cos^2(\varphi_1) \delta_{12} \, \mathrm{d}\theta_2 \, \mathrm{d}\theta_1 \, \mathrm{d}\omega_2 \, \mathrm{d}\omega_1, \tag{15}$$

where $$\delta_{12} = \begin{cases} 1 & \text{if } \omega_1 = \omega_2 \text{ and } \theta_1 = \theta_2 \\ 0 & \text{if } \omega_1 \neq \omega_2 \text{ and } \theta_1 \neq \theta_2. \end{cases} \tag{16}$$

THEORETICAL RESULTS

The theory derived in this paper is able to fully describe the mechanics of nonlinear sea waves interacting with a vertical seawall, by assuming the occurrence of an exceptionally large wave (either a high crest or a deep trough) of the surface displacement or of the wave pressure at a fixed point at a given time instant. As a result, the behaviour in space and in time of the nonlinear wave groups may be investigated by assuming the realisation of a very high amplitude H_C at the structure (y_0 = 0) or in front of it (y_0 < 0).

In detail, in this section, the deterministic closed-form solutions up to the second order of $\overline{\eta}_R$ and of $\overline{p}_{w_R}$ are applied in order to analyse the effects of nonlinearity when a very high crest amplitude H_C of the surface displacement is realised at time instant T = 0 at the structure (y_0 = 0) at (X, Y) = (0,0).

The theoretical solutions are evaluated by assuming for the directional wave spectrum of the incident waves given by the JONSWAP frequency spectrum (Hasselmann *et al*., 1973) with the directional spreading function of Mitsuyasu (Mitsuyasu *et al*., 1975).

By defining the dimensionless frequency $w = \omega / \omega_p$, with ω_p being the peak frequency of the spectrum, the JONSWAP spectrum may be expressed as:

$$E(\omega) = \alpha_{PH} g^2 \omega_p^{-5} w^{-5} \exp(-1.25 w^{-4}) \exp\left\{ \ln\gamma \exp\left[-\frac{(w-1)^2}{2\sigma^2} \right] \right\}, \tag{17}$$

where α_{PH} is the Phillip's parameter (ranging between 0.008 and 0.02 for wind waves), and γ and σ are the shape parameters. σ can be assumed to be equal to 0.08 and γ equal to 3.3 for the mean JONSWAP, and equal to 1 for the Pierson-Moskowitz spectrum (Pierson and Moskowitz, 1964).

As for the directional spreading function $D(\theta,\omega)$ of Mitsuyasu, its mathematical form is

$$D(\theta;\omega) = K(n) \left| \cos\left[\frac{1}{2}(\theta - \theta_{dom}) \right] \right|^{2n}, \tag{18}$$

where θ_{dom} is the angle between the *Y*-axis and the dominant direction of the spectrum, and *K*(*n*) is the normalizing factor,

$$K(n) = \left[\int_0^{2\pi} \cos^{2n}\left(\frac{1}{2}\theta\right) d\theta \right]^{-1}, \tag{19}$$

with *n* depending on the dimensionless wave frequency (such that $n = n_p w^5$ if $w \le 1$ and $n = n_p w^{-2.5}$ if $w > 1$), and on the fetch F_e and the wind speed *u* through the shape parameter $n_p = 7.5 \cdot 10^{-3} (gF_e / u^2)^{0.825}$.

In the applications we shall assume a Phillip's parameter α_{PH} equal to 0.012 and a parameter of the directional spreading function, n_p, equal to 25.

Effects of Ursell parameter

The effects associated with the frequency wave spectrum, the water depth and the wave steepness upon the nonlinear solution are evaluated next, using the Ursell number U_r, which is defined as

$$U_r = H_S / k_1^2 d^3 . \tag{20}$$

For the feature of wave groups at a seawall, in Eq. (20) H_S is the significant wave height of the incident waves, *d* the water depth at the seawall and k_1 is the wave number in deep water given by

$$k_1 = g^{-1} (2\pi / T_{m_{01}})^2 , \tag{21}$$

with $T_{m_{01}} = 2\pi\, m_0 / m_1$ the mean wave period related to the zeroth and the first-order moments of the frequency spectrum (the related wave length on deep water is $L_{m_{01}} = gT_{m_{01}}^2 /(2\pi)$).

The *j*-th moment m_j is

$$m_j = \int_0^{\infty} \omega^j E(\omega)\, \mathrm{d}\omega , \tag{22}$$

which, assuming the JONSWAP frequency spectrum, can be expressed as

$$m_j = \alpha_{PH} g^2 \omega_p^{-4+j} m_{w_j} , \tag{23}$$

being m_{w_j} the dimensionless moment:

$$m_{w_j} = \int_0^{\infty} w^{-5+j} \exp(-1.25 w^{-4}) \exp\left\{ \ln\gamma \exp\left[-\frac{(w-1)^2}{2\sigma^2} \right] \right\} \mathrm{d}w , \tag{24}$$

with $w = \omega / \omega_p$ dimensionless frequency and ω_p the peak frequency of the spectrum.

Thus, for the JONSWAP spectrum, using Eqs. (23) and (24), the mean wave period $T_{m_{01}}$ is made explicit as $T_{m_{01}} = T_p m_{w_0} / m_{w_1}$, and the following general relation between the significant wave height H_S and the peak period T_p ($\equiv 2\pi / \omega_p$) is introduced:

$$H_S = g\pi^{-2} T_p^2 (\alpha_{PH} m_{w_0})^{0.5} . \tag{25}$$

The Ursell number can be stated (Arena e Pavone, 2006) as

$$U_r = \frac{\alpha_{PH}^{0.5} m_{w_0}^{4.5}}{2\pi^3 m_{w_1}^4} \frac{1}{(d / L_{p_0})^3} . \tag{26}$$

In the last equation, d / L_{p_0} is the relative water depth, L_{p_0} is the wavelength on deep water related to the peak period ($L_{p_0} = gT_p^2 /(2\pi)$) and the ratio $m_{w_0}^{4.5} / m_{w_1}^4$ is equal to 0.16 for the Pierson-Moskowitz (γ=1) and 0.27 for the mean JONSWAP (γ=3.3).

The free-surface displacement and the wave pressure at some depth along the cross-section of the seawall are represented in the time domain in Figure 2 for three values of the Ursell number that are equal to 0.08, 0.01 and 0.004. The theoretical time series are evaluated at point $\underline{x}_0 + \underline{X} = 0$, assuming at

that point the occurrence of an exceptionally high crest H_C of $\bar{\eta}_{R_1}$, of elevation $4\sigma_R$ (see Eq. 7), at time instant T=0. The dominant direction of the spectrum with respect to the Y-axis is θ_{dom}=0, which implies that the wave groups approach the seawall orthogonally.

On the water surface profiles, the nonlinear component $\bar{\eta}_{R_2}$ is responsible for the increment in elevation of the highest crests and for the reduction in depth of the greatest troughs. The nonlinear water surface shows a significant asymmetry, with the heights of the highest crests exceeding the depths of the deepest troughs. The greatest nonlinear results are found for higher Ursell numbers (that is to say, at lower relative water depths d/L_{p0} for a fixed wave spectrum). At d/L_{p0} = 0.15, the highest crest is increased by a nonlinear contribution of about 36% and the deepest trough is reduced by about 24%, with respect to the linear prediction. When the water depth increases, these effects are reduced.

As regards the wave pressure on the time domain, the linear theory (lower panels of Figure 2, dotted lines) shows that the maxima exceed the minima at every water depth. Moreover, the positive peak of the process (absolute maximum) is always in phase with the maximum elevation at the surface. In other words, the positive peaks of the wave pressures to the first-order are realised when the highest crest H_C of the surface displacement occurs at time instant T = 0 at the structure.

The nonlinear theory strongly affects the behaviour of the wave pressure profiles in the time domain highlighting some of the main results at every Ursell number:

i) the absolute maxima of the nonlinear process (positive peaks) are reduced in elevation with respect to those produced using linear predictions; this difference decreases as the Ursell number is reduced;

ii) at the same time, the absolute minima of the nonlinear wave pressures (negative peaks) are significantly increased in depth with respect to those of the linear;

iii) as a consequence of *i*) and *ii*), the nonlinear profiles show a significant asymmetry between the positive and negative peaks, with the negative ones greatly exceeding the positive ones; finally, moving from the surface to the bottom, another important feature is found: at time instant T = 0, when the exceptionally high crest of $\bar{\eta}_R$ impacts the structure, a drop in pressure takes place,

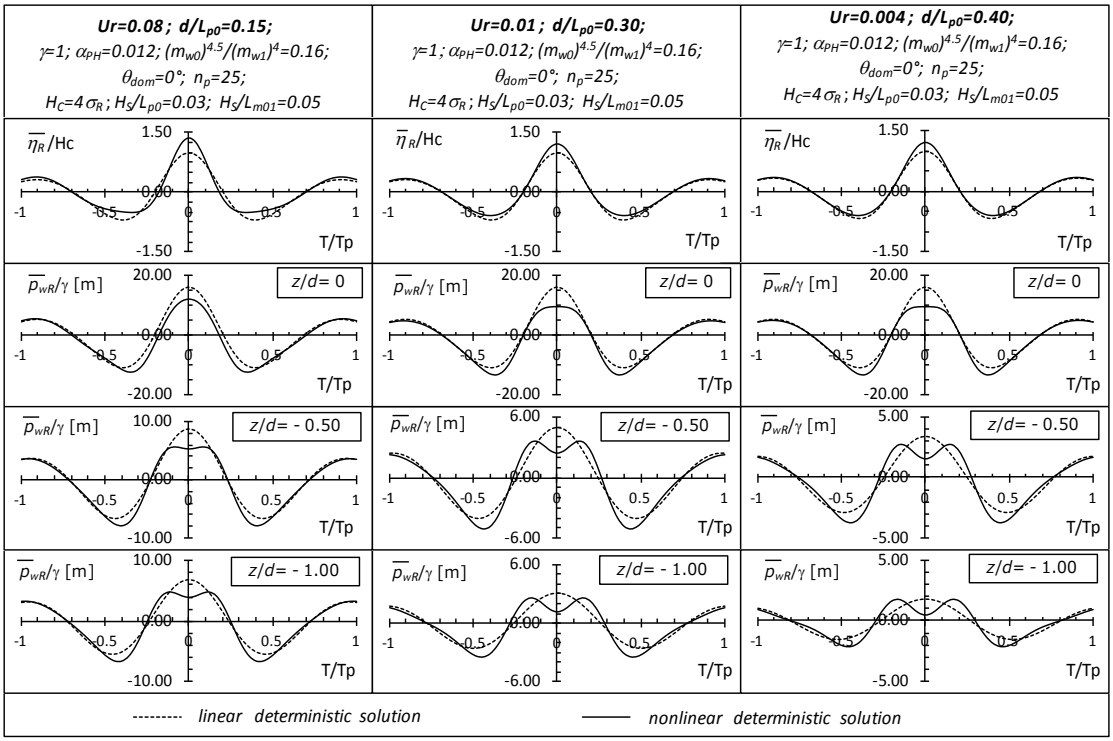

Figure 2. The surface displacement (upper panels) and the wave pressures at different depths, z/d, along the cross section of the structure are represented to the first-order (dotted lines) and up to the second-order (continuous lines) in time domain for different Ursell number, U_r, by assuming a Pierson-Moskowitz-Mitsuyasu directional wave spectrum. The theoretical time series are achieved by assuming the occurrence of an exceptionally high crest, H_C, of the surface displacement $\bar{\eta}_R$ at T=0 at x_0+ X = 0.

with the appearance of characteristic double-humped profiles. Two maxima (positive peaks) of the nonlinear wave pressure are produced that are equal in value and out of phase with the maximum elevation at the surface; they occur before and after the realisation of the highest wave crests of the surface waves.

These results of nonlinearity on wave pressures were evaluated by defining a number of characteristic parameters, which are represented versus the relative water depth d/L_{p0} in Figure 3, for two different dominant wave directions θ_{dom} (coinciding with the wave group propagation with respect to the *Y*-axis) equal to 0° and 30° and for the Pierson-Moskowitz and a mean JONSWAP frequency spectrum. The theoretical results were computed assuming the occurrence of the highest crest of the surface displacement ($H_C = 4\sigma_R$) at point (X, Y) = (0,0) at time instant T = 0.

We focus the attention on the absolute maximum of the linear wave pressure, which is $\overline{p}_{w_{R1-\max}}$. That is always realised at time instant T=0 of the highest elevation of the surface waves at the seawall, while the absolute maximum of the nonlinear process may occur at some time before T=0, depending upon the wave conditions. Thus, we considered $\overline{p}_{w_{R-\max}}$, which is the absolute maximum of the nonlinear wave pressure and, moreover, the second-order wave pressure at T=0, that is $\overline{p}_{w_{R-\max}}(T=0)$. Through these different quantities, some characteristic parameters describing the effects of nonlinearity on wave pressures at the seawall are introduced, which are shown versus d/L_{p0} in Figure 3.

First, we will focus upon the dominant wave direction when it is equal to zero (see the left-hand side of Figure 3). In considering the results in panel (a.1) in Figure 3, we observe that at z/d=–0.3, the nonlinear positive peaks of the wave pressures are always smaller than those produced using a linear solution. When d/L_{p0} is greater than 0.15, the nonlinear theory reduces the positive peaks by about 30%.

Moving from the surface towards the bottom (z/d=–1), this trend is maintained only for lower d/L_{p0}. An important result is thus found: at z/d=–1 for increasing water depth d/L_{p0}, the maxima of the nonlinear wave pressures increase constantly, and at a deeper water depth, they become of the same order of magnitude as those achieved using a linear approach.

We said earlier that the highest crest of surface waves impacts the seawall at time instant T =0, at which point the nonlinear theory would predict a drop in the wave pressure, while the greatest maximum of the process will occur a few times before and after T=0. In panel (c.1) it is evident that the nonlinear wave pressure at T=0 regularly turns out to be smaller than its maximum, with the greatest differences taking place at the deepest depths. For example, at the bottom depth, the absolute maxima of the nonlinear wave pressure are greater than 4 times that one realized at time instant T=0, assuming the Pierson-Moskowitz frequency spectrum. Therefore, the theory up to the second-order highlights the fact that, when wave groups impact the structure orthogonally, the realisation of the maximum elevation on the surface corresponds to a strong attenuation of the wave pressures at the seawall (see panel (b.1)).

Near the surface, at z/d=–0.3, the wave pressure up to the second-order is about half of that predicted using a linear solution. At the bottom, the linear wave pressures are reduced by the second-order contributions by up to 75% for the Pierson-Moskowitz spectrum and by up to 90% for a mean JONSWAP spectrum, since the nonlinear wave pressures approach zero.

As regards the nonlinear negative peaks (panel (e.1)), it was found that at the bottom they are about 1.30 times those of the positive peaks for every water depth for the Pierson-Moskowitz spectrum, and increase by about 23% when the frequency spectrum is the mean JONSWAP. For a lower depth (at z/d=–0.3), this trend is maintained, with the exception of a lower depth. Thus, it is confirmed that the nonlinear theory predicts a wave pressure process characterised by a strong asymmetry, with the depth of the deepest troughs significantly exceeding the heights of the highest crests. This result is due mainly to the fact that, for wave groups in reflection, the theory that is exact to the second-order underlines the fact that the deepest troughs are strongly increased with respect to the linear solution (panel (d.1)) by about 30%, and up to 70% in deep water at the bottom depth for a narrower frequency spectrum.

Comparing the results in the left- and right-hand sides of Figure 3, we observe that the influence of the dominant wave direction θ_{dom} is exerted mainly on the positive maxima of the wave pressures. From panels (a.2), (b.2) and (c.2) it is clear that, for increasing values of $|\theta_{dom}|$, the greatest maximum of the nonlinear wave pressure occurs at the instant T=0, in phase with the highest crests of the surface waves, and at the same time instant of the greatest linear wave pressure at the seawall. That is the main results

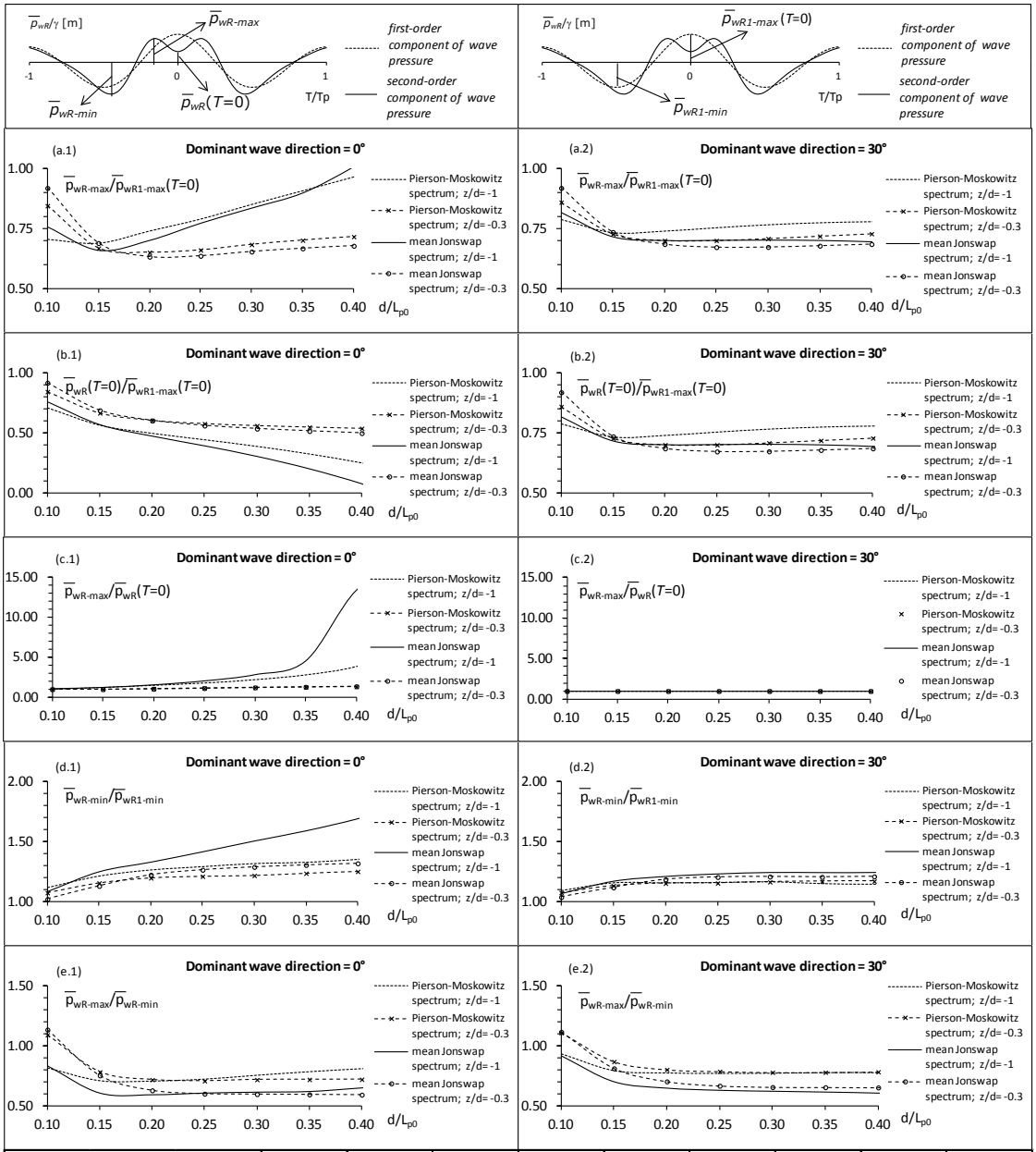

d/L_{p0}	0.10	0.15	0.20	0.25	0.30	0.35	0.40	0.45	0.50
Ur - Pierson-Moskowitz spectrum	0.28	0.084	0.035	0.018	0.010	0.007	0.004	0.003	0.002
Ur - mean Jonswap spectrum	0.48	0.142	0.060	0.031	0.018	0.011	0.007	0.005	0.004

Figure 3 . Some characteristic parameters describing the effects of nonlinearity on wave pressures at the seawall are shown versus the relative water depth d/L_{p0}. For all quantities make reference to the upper panels. The theoretical results are achieved by assuming the occurrence of an exceptionally high crest, of elevation $H_C=4\sigma_R$, of the surface displacement, η_R, at time T=0 at $x_0+X=0$.

associated to the change of θ_{dom} .

Effects of wave direction

In Figure 4, on the left-hand side, a comparison of the nonlinear water surface $\overline{\eta}_R = \overline{\eta}_{R_1} + \overline{\eta}_{R_2}$ and wave pressure $\overline{p}_{w_R} = \overline{p}_{w_{R_1}} + \overline{p}_{w_{R_2}}$ in the time domain is shown; it considers wave groups that are approaching the structure orthogonally (θ_{dom}=0, dotted lines), with the direction of their advance making an angle of 30° with respect to the *Y*-axis (θ_{dom}=30°, continuous lines). The theoretical time series are relative to a water depth, d/L_{p0}, that is equal to 0.15, with an Ursell number equal to 0.08.

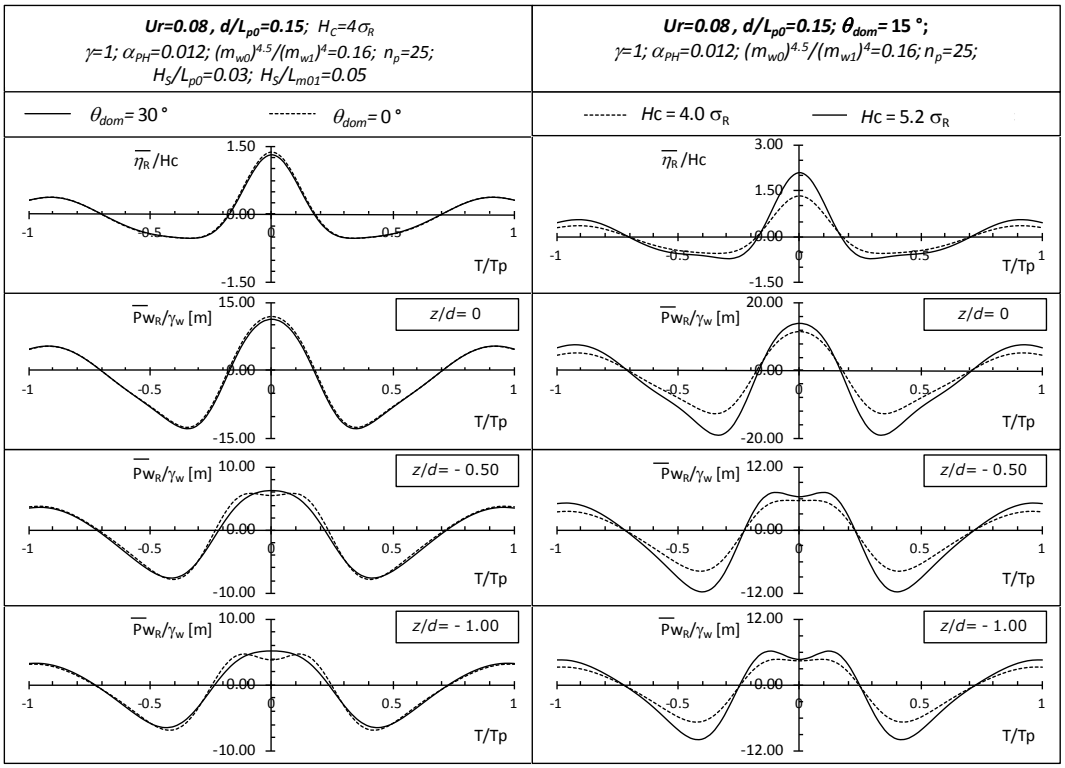

Figure 4. The nonlinear free surface displacement (upper panels) and the nonlinear wave pressures at different depths along the cross section of the structure are represented in time domain. In the left-hand side, the effects of dominant wave direction are investigated, the second-order profiles for θ_{dom}=0° (dotted lines) and for θ_{dom}=30° (continuous lines) are shown. In the right-hand side, the profiles when H_C goes from 4.0σ_R to 5.2σ_R are illustrated.

They were computed by assuming the occurrence of an exceptionally high crest H_C of $\bar{\eta}_R$ at time instant T=0 at the point $\underline{x}_0 + \underline{X} = 0$.

The comparison points out that the directionality does not influence the behaviour of the surface displacement. With the nonlinear wave pressures, the directionality is mainly responsible for the disappearance of the humped profiles, with the realisation of the local minimum at time instant T=0, which is preceded and followed by two absolute maxima. For dominant wave direction in absolute value greater than zero, the highest maximum of the nonlinear pressure is realised at time instant T=0, in phase with the occurrence of the highest crest of the surface waves at the seawall.

Finally, it is well known that nonlinear effects are amplified for larger wave steepness. It is interesting to observe that for a dominant wave direction different from zero, when, for fixed wave conditions, the high crest H_C of the surface waves at the seawall increases, the nonlinear effects are more remarkable, both on the surface displacement and on the wave pressures. This results is shown on the right-hand side of Figure 4 for d/L_{p0}=0.15 with θ_{dom}=15°, when H_C goes from 4.0σ_R to 5.2σ_R.

VALIDATION OF NONLINEAR THEORY WITH A SMALL-SCALE FIELD EXPERIMENT

Description of experiment

The nonlinear theory for sea wave groups interacting with a vertical seawall that is proposed in this paper was validated in a small-scale field experiment carried out at the Natural Ocean Engineering Laboratory (NOEL) in Reggio Calabria (Italy). In this laboratory, located on the waterfront of Reggio Calabria on the east coast of the Strait of Messina, it is possible to carry out experiments directly in the sea using techniques associated with the laboratory tanks (Boccotti *et al*. (1993, 2012), Boccotti (2000).

A small fully reflective upright seawall with a frame set in reinforced concrete was built. The structure, which consisted of 9 caissons, had a total length of 16.2 m and a height of 3.0 m, and was placed at a depth of 1.9 m with respect to the mean water level (MWL). 16 pressure transducers were placed on the sea-beaten side along the vertical cross section of the central caisson forming the seawall, in order to measure the fluctuation of the wave pressures acting on it (the layout of the instruments is shown in Figure 5). The incident waves (in the undisturbed field) were evaluated by means of two

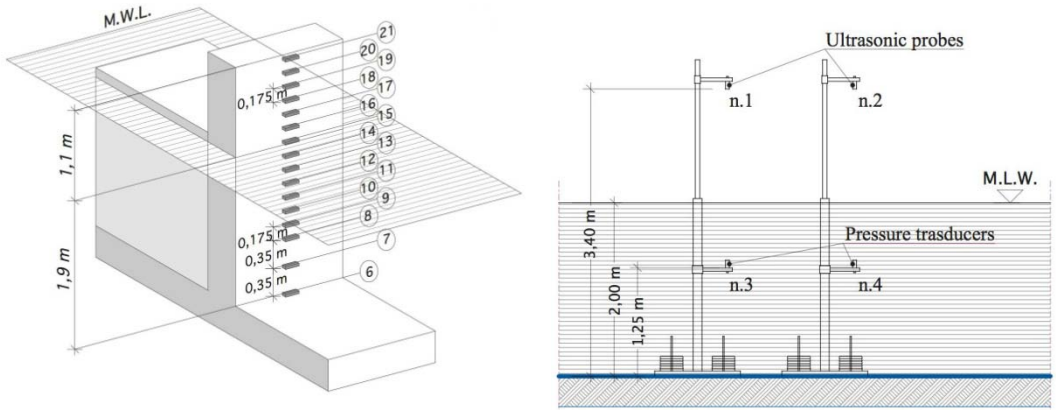

Figure 5. Field experiment carried out on the sea of Reggio Calabria in the NOEL laboratory: map of the gauges at the structure (left-hand side) and on the piles in an undisturbed field (right-hand side) are shown.

ultrasonic probes and two pressure transducers. One of each instrument was assembled on a thin pile with a diameter of 0.05 m, and was positioned 13 m from the seawall (Figure 5).

Each gauge recorded continuously for five minutes at a sampling rate of 10Hz. Among all records, only those of pure wind waves without overturning or breaking waves were considered in the present analyses. In all, there were 94 records that were characterised by the following wave conditions: significant wave height H_S in the undisturbed field, between 0.21m and 0.41m, and peak period T_p between 1.9s and 2.7s. Thus, the relative water depth was $0.16 \leq d/L_{p0} \leq 0.32$.

The considered records represent, in a hydraulic Froude similitude, a small-scale model of sea states during severe storms. Because of the change in the mean water level caused by the tide, the water depth d ranged between 1.76m and 1.95m. The dominant wave direction θ_{dom} had a range of [-9°, 15°] and it was positive when clockwise with respect to the normal outgoing to the structure. In the analysed records, the spectral shape in the frequency domain was evaluated using Boccotti's ψ^* narrow bandedness parameter (Boccotti 1982, 2000), defined as

$$\psi^* = \left|\psi(T^*)/\psi(0)\right|, \tag{27}$$

which is the quotient between the absolute value of the first minimum, that occurs at $T = T^*$, and the absolute maximum of the autocovariance function. The values of ψ^* range in $(0,1)$: it is equal to 1 for an infinitely narrow spectrum, 0.73 for a mean JONSWAP spectrum and 0.65 for a Pierson-Moskowitz spectrum. In the 94 records that were considered, ψ^* was within $(0.65, 0.76)$ at the surface, and the Ursell number varied from 0.08 to 0.01.

Comparison between theoretical and experimental results

The 94 records considered for validation of the theory are identified by a full sea wave reflection given by the seawall, and by the resulting pattern of standing wave groups close to the structure.

In this section, the nonlinear theory is tested by considering as input in the theoretical computations the values of the wave parameters, such as the significant wave height H_S, the peak period T_p, the tide level, the dominant wave direction θ_{dom} and the relative water depth d/L_{p0} of the record being compared. As regards the theoretical directional spectrum, the JONSWAP-Mitsuyasu spectrum is assumed, with spectral shape parameters γ such that ψ^* parameter related to the theoretical spectrum is equal to the one of the considered records.

The theory can be applied when either an exceptionally high crest H_C or trough H_T of the surface displacement is realised. It is noteworthy to observe that a positive (absolute maximum) or negative (absolute minimum) peak of the wave pressure at the bottom of the seawall may be produced by the occurrence on the surface of either an exceptionally high crest amplitude H_C or trough amplitude H_T of the surface displacement.

Figures 6–8 present a number of comparisons between the theoretical and analytical results. In each figure, lower panels represent the wave pressures in the time domain at the depth of the pressure transducers assembled along the cross section of the tested seawall (see Figure 5); the dots are the measurements given by the gauges and the continuous lines are the theoretical profiles that are exact to

Table 1. Wave field conditions of the five records of the experiment during which the greatest peaks of the process occurred.

Record	$\alpha = p_{w_6} / \sigma_{p_{w_6}}$	$\sigma_{p_{w_6}}(m)$	H_S (m)	T_p (s)	Tide (m)	θ_{dom} (deg)	d / L_{p0}	$\psi^*[z=0]$	U_r
1	3.37	0.0788	0.41	2.54	-0.06	0	0.18	0.66	0.07
2	3.17	0.0571	0.31	2.37	-0.05	8	0.21	0.65	0.04
3	-5.62	0.0444	0.31	2.21	-0.05	3	0.24	0.67	0.03

the second order. The second-order analytical profiles were computed by assuming the occurrence of either a very high wave crest H_C or a wave trough H_T of the surface displacement, such that the absolute maximum (or minimum) of the analytical wave pressures at the bottom depth turns out to be equal in value to the one recorded by gauge n°6. The instants of the wave crests of the surface waves at the structure were identified by the signals transmitted by the upper pressure transducers. Therefore, in Figures 6–8, only the nonlinear water elevation that is computed using the theory is shown. Moreover, the recorded wave force per unit length at the midsection of the structure, which is computed by the integration of the measured wave pressures at different water depths, is depicted (in the upper panels, by dots). The theoretical wave force (upper panels, a continuous line) is computed by considering the following. *i*) During the crest elevation phase of the water surface, a linear trend was assumed between the total wave pressure up to the second order at the mean water level and the nonlinear wave elevation of the free-surface displacement. *ii*) During the trough amplitude phase of the water surface, the pressure was assumed to be equal to the hydrostatic pressure if it was greater than the nonlinear wave pressure.

Figures 6 and 7 show the records of the experiment, in which the two highest positive peaks of the wave pressure process at the bottom $p_{w_6} / \sigma_{p_{w_6}}$, are realised ($\sigma_{p_{w_6}}$ being the standard deviation of the wave pressure p_{w_6} recorded at the bottom depth by gauge n°6). Figure 8 refers to the first negative peak of the $p_{w_6} / \sigma_{p_{w_6}}$ process.

For the comparisons shown in Figures 6 and 7, the theory was applied by assuming the realisation of an exceptionally high crest H_C of $\overline{\eta}_R$ at time instant t = 0 at the structure. Records 1 and 2, which are analysed in Figures 6 and 7, are almost homogenous in terms of wave characteristics, except for the dominant wave direction, which is null for record number 1 and greater than zero for record number 2 (see Table 2). The recorded time series in Figures 6 and 7 are centred (t = 0) at the time instant of the maximum elevation measured at the seawall on the surface. For the comparisons between the analytical and experimental results, we supposed at the same time instant the occurrence of an exceptionally high crest H_C of the theoretical nonlinear surface displacement (that is, H_C equal to $4.54\sigma_R$ and $3.84\sigma_R$, respectively, for records 1 and 2, with σ_R being the standard deviation of the measured surface waves at the seawall). As predicted by the nonlinear theory (see Figures 2 and 4), when the wave groups approach the structure orthogonally (the dominant wave direction θ_{dom} is zero) the greatest maximum of the wave pressures beneath the mean water level is out of phase with respect to the highest elevation on the surface, at which a local minimum of the wave pressures is realised. This phenomenon can be seen in record 1 (the dots in Figures 6). If we focus upon the recorded wave pressure at the bottom depth (gauge n°6), we find that the process is a very asymmetric, with the highest maximum being about 0.82 times the greatest minimum. The differences between the positive peak of the wave pressure and the wave pressure at the time instant of the highest elevation at the surface is quite important; in the record 1 the positive peak exceeds the pressure by about 56% at time instant t = 0. The theory up to the second order (the continuous lines in Figure 6) shows a very good agreement with the experimental data in terms of both trends and values, close to the realisation of the exceptionally high crest of water displacement. The theory is able to fully describe the main phenomena under the mean water level; namely the drop in pressure at t=0, and the highest maximum being out of phase with the maximum elevation at the surface. Above the mean water level, a number of differences are found in the predictions of the highest elevation with respect to the experimental data; in this case the theoretical results are more conservative with regard to positive extreme values.

In record 2, even though it is characterised by an Ursell number smaller than those in record 1, the wave groups show a direction of advance equal to 8° with respect to normal to the seawall. According to the nonlinear theory, the recorded wave pressure profiles under the mean water level are smooth, without the formation of two humps (the dots in Figure 7). The absolute maximum of the recorded wave

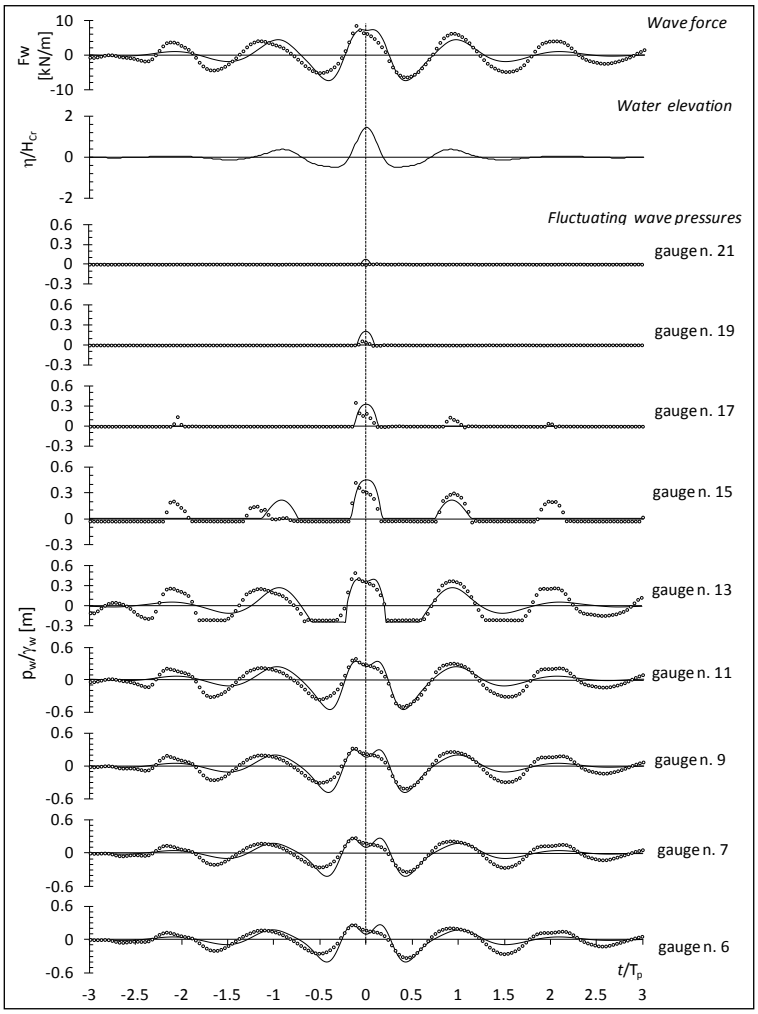

Figure 6. Record n.1 of Table 1 . The recorded time series (dots) are centred at time instant of the highest elevation on the surface at seawall. The theoretical second-order wave pressures (continuous lines) are computed at every depth by assuming at the previous time instant the occurrence at the structure of an exceptional high crest $H_C(=4.54\sigma_R)$ of the surface displacement.

pressures is in phase with the maximum water elevation along the cross section of the seawall. The wave pressures turn out to describe a peculiar asymmetry with greater minima in this case as well; at the bottom (gauge n°6) the ratio between the positive and negative peaks of the measured wave pressures is equal to 0.73. The nonlinear theory (the continuous lines in Figure 9) fully agrees with the experimental data, as it is able to describe all the results highlighted here.

Finally, Figure 8 presents the record where the greatest negative peaks of the wave pressure at the bottom (gauge n°6) occurred during the experiment. The record are centred (t = 0) at the time instant of the realisation of the greatest minimum of wave pressure at the seawall at the bottom depth. In our application of the nonlinear theory, we have supposed at the same time instant the occurrence of an exceptionally high trough H_T of the theoretical nonlinear surface displacement (that is, H_T equal to $3.74\sigma_R$, with σ_R being the standard deviation of the measured surface waves at the seawall). With respect to records 1 and 2, an enhancement of the asymmetry of the wave pressure profiles is found. The deepest troughs are about twice as deep as the heights of the highest crests of the wave pressures in records 1 and record 2.

Figure 8 considers record 3 (see Table 2), which was identified as having one of the lowest Ursell number values recorded during the experiment, and by a θ_{dom} close to zero. From the signals of the highest gauges (dots in Figure 8) we recognise the realisation of two crests of surface waves at the seawall at time instants $t = -0.43T_p$ and $t = 0.48T_p$, respectively, for gauge n. 17, which are before and after the occurrence of the deepest trough of the surface waves, which is fixed at time instant t = 0. For each of these wave crests on the surface, the formation of humped profiles on the wave pressures is observed at the lower gauges, with the positive peaks being out of phase with the highest elevation of

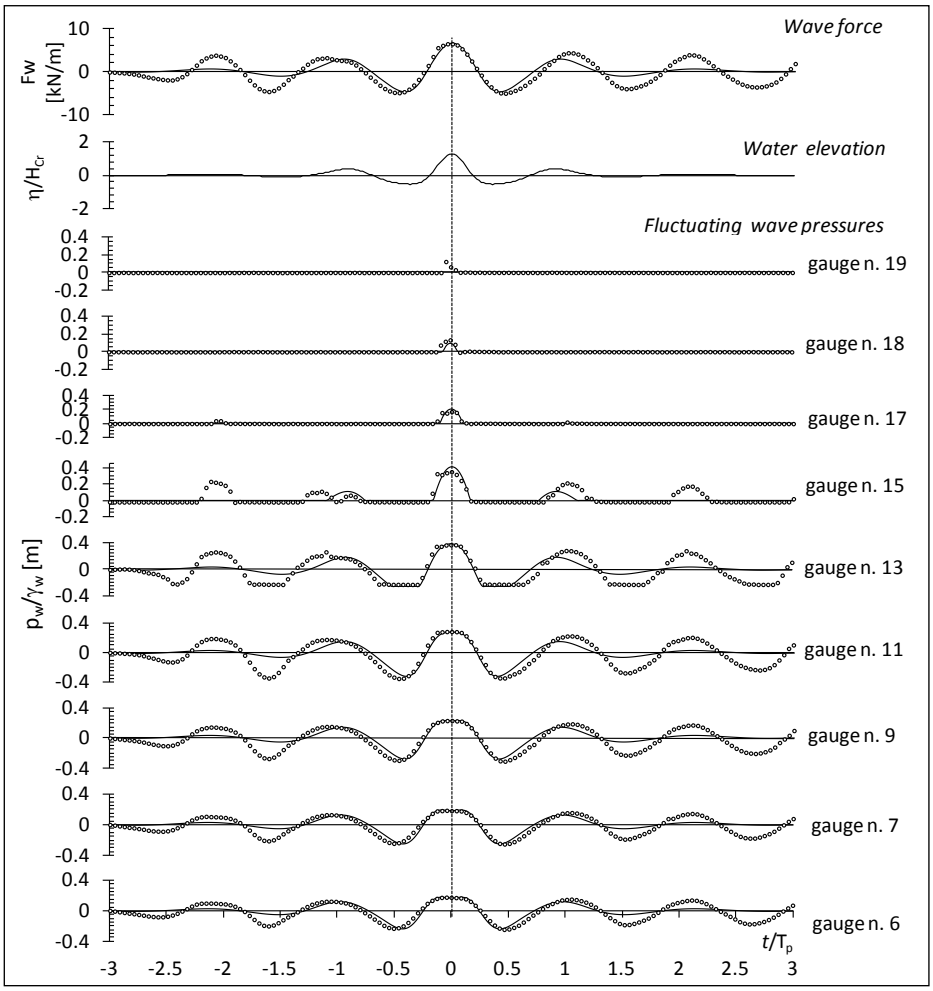

Figure 7. Record n.2 of Table 1. The recorded time series (dots) are centred at time instant when the absolute maximum of the measured wave pressure occurs at bottom. By assuming at the same time instant the occurrence at the structure of an exceptional high crest $H_C(=3.84\sigma_R)$ of the surface displacement, the theoretical second-order wave pressures (continuous lines) are computed at every depth.

the upper gauges. These peaks occur, for gauge n. 6, at $\pm 0.61T_p$, and the drop in the positive pressure is quite important: the ratio between the greatest positive pressure (at $t=\pm 0.61T_p$) and the positive pressure at the time of the highest crest of the surface waves is about 2.6 in both cases. The theory up to the second order (the continuous lines in Figure 8) is able to well describe the characteristics of the record, in terms of both the positive and negative peaks of the wave pressure in a process characterised by asymmetry.

Finally, Figure 9 shows, for every record in the experiment, the ratio (upper panel) between the wave pressures recorded by gauges n°12 and n°6 at time instant $\underline{t}$, when the highest maximum of the wave pressure at gauge n°12 (located above the mean water level) is realised; in the lower panel, the ratio between the maximum positive wave pressures recorded by gauges n°12 and n°6 is shown (the two maxima may occur at different time instants, depending upon the wave conditions). These behaviours confirm the distinct phenomenon predicted by nonlinear theory (Table 1): that is the strong reduction in wave pressure at the bottom depth corresponds to the realisation of the greatest positive peak on the surface when the dominant direction of advance of the wave groups is zero, while under the same conditions, the absolute positive maxima varies gradually along the cross section of the seawall. This effect is enhanced as the relative water depth increases. For example, at d/L_{p0} = 0.3, the highest maximum recorded at gauge n°12 was 6.2 times the positive pressure recorded at the same time instant at the bottom, and 2.5 times the highest maximum recorded at gauge n°6. This trend is distinct for θ_{dom}=0. For increasing values of $|\theta_{dom}|$, the quotient between the highest positive maximum realised on the surface steadily remains about twice the quotient recorded at the bottom. This parameter is about equal in value if we consider the variation of the absolute maxima along the cross section of the seawall

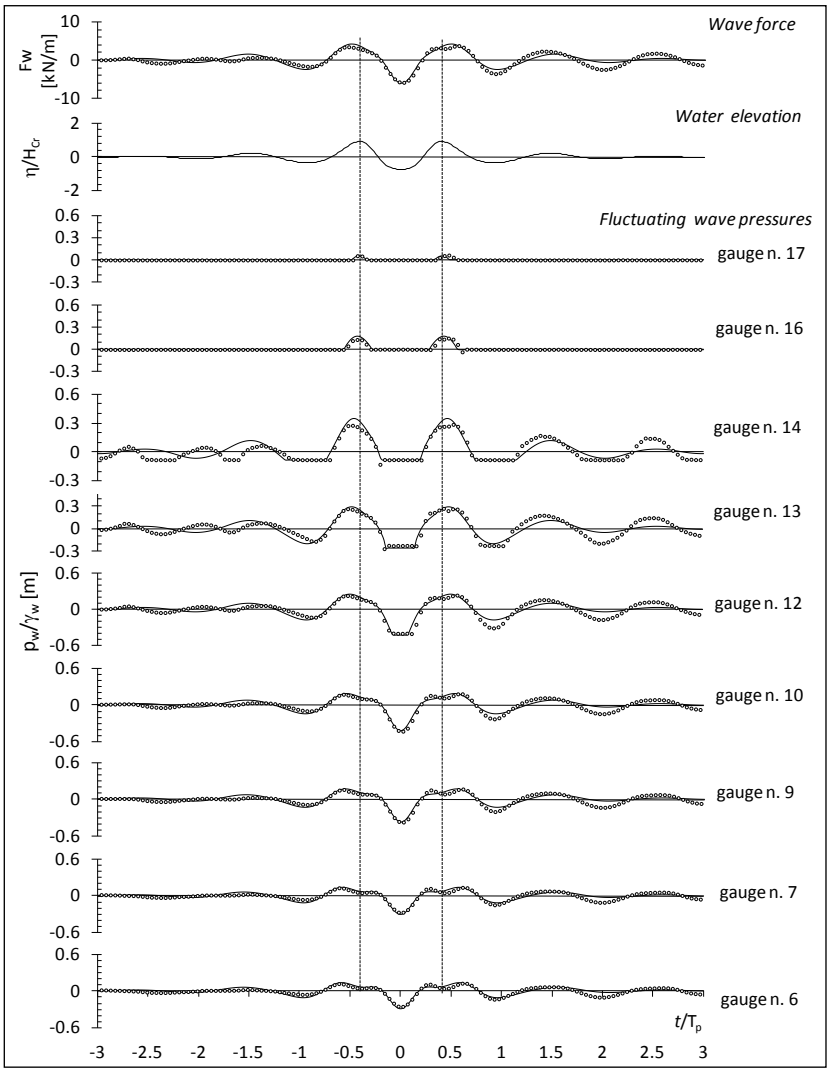

Figure 8. Record n.3 of Table 1. The recorded time series (dots) are centred at time instant when the absolute minimum of the measured wave pressure occurs at bottom. By assuming at the same time instant the occurrence at the structure of an exceptional high trough $H_T(=3.74\sigma_R)$ of the surface displacement, the theoretical second-order wave pressures (continuous lines) are computed at every depth.

(see both panels in Figure 9). This confirms the fact that, for all the data collected during the experiment when θ_{dom} differs from zero, the greatest positive maximum at the bottom is in phase with the highest positive maximum on the surface.

CONCLUSIONS

In this paper, an analytical close-form solution was derived, up to the second order, for three-dimensional wave groups that are fully reflected by an upright seawall. The theory revealed that the second-order contributions strongly affect the mechanics of wave groups when an exceptionally high crest or deep trough of the free-surface displacement process impacts the structure, both on the water surface and on the wave pressure acting on the structure. Distinctive phenomena of nonlinearity has been identified on the wave pressures in time domain, which are strongly influenced by the wave conditions.

The proposed nonlinear theory for three-dimensional wave groups interacting with a vertical seawall in the absence of overturning or breaking waves was tested using data from a small-scale field experiment carried out at the Natural Ocean Engineering Laboratory in Reggio Calabria (Italy)., demonstrating that the theory is able to capture the main distinctive phenomena that characterise the nonhomogeneous wave field of very high wave groups at a seawall, which can be associated with the effects of nonlinearity.

APPENDIX

$$A_n^- = g\omega_1^{-1}\omega_2^{-1}\{B_n^- - k_1k_2[-(-1)^n\cos(\theta_1+(-1)^n\theta_2)+\tanh(k_1d)\tanh(k_2d)]\}+(\omega_1^2+\omega_2^2)/g$$
$$A_n^+ = g\omega_1^{-1}\omega_2^{-1}\{B_n^+ - k_1k_2[-(-1)^n\cos(\theta_1+(-1)^n\theta_2)-\tanh(k_1d)\tanh(k_2d)]\}+(\omega_1^2+\omega_2^2)/g \quad \text{(A-1)}$$

$$C_n^- = B_n^-\frac{\cosh[|\underline{\mathbf{k}}_n^-|(d+z)]}{\cosh(|\underline{\mathbf{k}}_n^-|d)}; \qquad C_n^+ = B_n^+\frac{\cosh[|\underline{\mathbf{k}}_n^+|(d+z)]}{\cosh(|\underline{\mathbf{k}}_n^+|d)} \quad \text{(A-2)}$$

$$B_n^- = \frac{(\omega_1-\omega_2)\{\omega_2k_1^2[1-\tanh^2(k_1d)]-\omega_1k_2^2[1-\tanh^2(k_2d)]\}+2(\omega_1-\omega_2)^2k_1k_2\{\tanh(k_1d)\tanh(k_2d)-(-1)^n\cos[\theta_1+(-1)^n\theta_2]\}}{(\omega_1-\omega_2)^2-g|\underline{\mathbf{k}}_n^-|\tanh(|\underline{\mathbf{k}}_n^-|d)}$$

$$B_n^+ = \frac{(\omega_1+\omega_2)\{\omega_2k_1^2[1-\tanh^2(k_1d)]+\omega_1k_2^2[1-\tanh^2(k_2d)]\}-2(\omega_1+\omega_2)^2k_1k_2\{\tanh(k_1d)\tanh(k_2d)+(-1)^n\cos[\theta_1+(-1)^n\theta_2]\}}{(\omega_1+\omega_2)^2-g|\underline{\mathbf{k}}_n^+|\tanh(|\underline{\mathbf{k}}_n^+|d)}$$

n=1,2 (A-3)

$$\underline{\mathbf{k}}_n^- = (k_1\sin\theta_1-k_2\sin\theta_2;\ k_1\cos\theta_1+(-1)^nk_2\sin\theta_2); \quad \underline{\mathbf{k}}_n^+ = (k_1\sin\theta_1+k_2\sin\theta_2;\ k_1\cos\theta_1-(-1)^nk_2\sin\theta_2). \quad \text{(A-4)}$$

REFERENCES

Arena F., 2005. On non-linear very large sea wave groups, Ocean Eng. 32, 1311–1331.

Arena, F., 2006. Interaction between long-crested random waves and a submerged horizontal cylinder, *Phys. Fluids*, 18, 076602

Arena F., Ascanelli A., Nava V., Pavone D., Romolo A., 2008. Non-linear three-dimensional wave groups in finite water depth, Coastal Eng. 55, 1052-1061.

Arena F. and Pavone D., 2006. The return period of non-linear high wave crests, J. Geophys. Res. 111, C8, paper C08004.

Boccotti P., 1982. On ocean waves with high crests, Meccanica 17, 16-19.

Boccotti P, 1997. A general theory of three-dimensional wave groups. Part I: the formal derivation. Part II: interaction with a breakwater, Ocean Eng. 24, 265-300.

Boccotti P., 2000. Wave Mechanics for Ocean Engineering. Elsevier Science, New York.

Boccotti P, Barbaro G., Mannino L., 1993. A field experiment on the mechanics of irregular gravity waves, J. Fluid Mech. 252, 173-186.

Boccotti, P., Arena, F., Fiamma, V., Romolo, A. & Barbaro, G., 2011. Estimation of mean spectral directions in random seas, *Ocean Engineering*, 38, 509-518, ISSN: 0029-8018.

Boccotti, P., Arena, F., Fiamma, V., Romolo, A. & Barbaro G., 2012. A small scale field experiment on wave forces on upright breakwaters, *Journal of waterway port coastal and ocean engineering-ASCE*, 138, 97-114, ISSN: 0733-950X

Cooker M.J., Peregrine D.H., 1995. Pressure impulse theory for liquid impact problems, J. Fluid Mech. 297, 193-214.

Fultz D., 1962. An experimental note on finite-amplitude standing gravity waves, J. Fluid Mech. 13, 193-212.

Goda Y., 1967. The fourth order approximation to the pressure of standing waves, Coast. Engrg. in Japan 10, 1-11.

Hasselmann K., Barnett T.P., Bouws E., Carlson H., Cartwright D.E., Enke E., Ewing J.A., Gienapp H., Hasselmann D.E., Krusemann P., Meerburg A., Müller P., Olbers D.J., Richter K., Sell W., Walden H., 1973. Measurements of wind-wave growth and swell decay during the Joint North Sea Wave Project (JONSWAP) Dtsch. Hydrogr. Z. A12, 1-95.

Longuet-Higgins M.S., 2001. Vertical jets from standing waves. Proc. R. Soc. London Ser. A 457, 495-510.

Longuet-Higgins M.S., Dommermuth D.G., 2001. Vertical jets from standing waves. II, Proc. R. Soc. London A 457, 2137-2149.

Mitsuyasu H., Tasai F., Suara T., 1975. Observation of directional spectrum of ocean waves using a clover-leaf buoy, J. Phys. Oceanogr. 5, 750-760.

Jiang L., Ting C.-L., Perlin M., Schultz W.W., 1996. Moderate and steep Faraday waves: instabilities, modulation and temporal asymmetries, J. Fluid Mech. 329, 275-307.

Ohl, C. O. G., Taylor, P. H., Eatock Taylor, R., and Borthwick, A. G. L., 2001. Water wave diffraction by a cylinder array. Part 2. Irregular waves, *J.Fluid Mech*. 442, 33.

Penney W.G., Price A.T., 1952. Finite periodic stationary gravity waves in a perfect fluid Part II, Philos. Trans. R. Sot. London Ser. A 244 882, 254-284.

Peregrine D.H., 2003. Water-wave impact on walls, Ann. Rev. Fluid Mech. 35, 23-43.

Pierson W.J., Moskowitz L.A., 1964. A Proposed Spectral Form for Fully Developed Waves Based on the Similarity Theory of S. A. Kitaigorodskii, J. Geophys. Res. 69, 5181-5190.

Romolo A., Arena F., 2008. Mechanics of nonlinear random wave groups interacting with a vertical wall, Phys. Fluids. 20, 1-16.

Romolo A., Malara G., Barbaro G., Arena F., 2009. An Analytical Approach for the Calculation of Random Wave Forces on Submerged Tunnels. *Applied Ocean Research*, 31; 31-36, ISSN: 0141-1187, doi: 10.1016/j.apor.2009.04.001

Romolo A., Arena F. 2010 A Small-Scale Field Experiment for the Validation of a Theory on Reflection of Nonlinear Short-Crested Wave Groups. *Proc. 32st International Conference On Coastal Engineering* (ICCE 2010) - ASCE, Shanghai, China, 30 June - 5 July 2010, paper no. waves.58.

Sharma J.N. , Dean R.G., 1981. Second-order directional seas and associated wave forces, Soc Pet. Eng. J. 4, 129.

Schultz W.W., Vanden-Broeck J.-M., Jiang L., Perlin M., 1998. Highly nonlinear standing water waves with small capillary effect, J. Fluid Mech. 369, 253-272.

Schwartz L.W., Fenton J.D., 1982. Strongly nonlinear waves, Ann. Rev. Fluid Mech. 14, 39-60.

Tadjbakhsh I., Keller J.B., 1960. Standing surface waves of finite amplitude, J. Fluid Mech. 8, 442-451.

Taylor G.I., 1953. An experimental study of standing waves, Proc. R. Soc. Lond. A 218, 44-59.

Tsai C.-P., Jeng D.-S., 1994. Numerical Fourier solutions of standing waves in finite water depth, Appl. Oc. Res. 16, 185-193.

Walker, D. A. G. and Eatock Taylor, R., 2005. Wave diffraction from linear arrays of cylinders, *Ocean Eng*., 32, 2053.